APPENDIX 13

COULOMB 3.1 RE-INTERPRETED STRESS MODELING
IN DIXIE VALLEY, NEVADA

Table of Contents

List of Figures

List of Tables

Modeling fault-induced stress and strain near Dixie Valley Geothermal Field, NV

Authors: Maisie Nichols and Trenton Cladouhos, AltaRock Energy Inc.

Background

The Dixie Valley Geothermal Field (DVGF) sits within Dixie Valley, Nevada (Figure 1) located in the western Great Basin region of the extensional Basin and Range Province. The valley is bounded by normal faults that have produced several large earthquakes over the past ~3000 years, including the 2-2.5 ka "Gap" Earthquake along the Stillwater Gap Segment (SGS) of the Dixie Valley Fault (DVF), the 1915 Pleasant Valley Earthquake along the Pleasant Valley Fault (PVF), and 1954 Dixie Valley Earthquake along the southern section of the DVF. These earthquakes influence the stress and strain distribution throughout the region surrounding the DVGF.

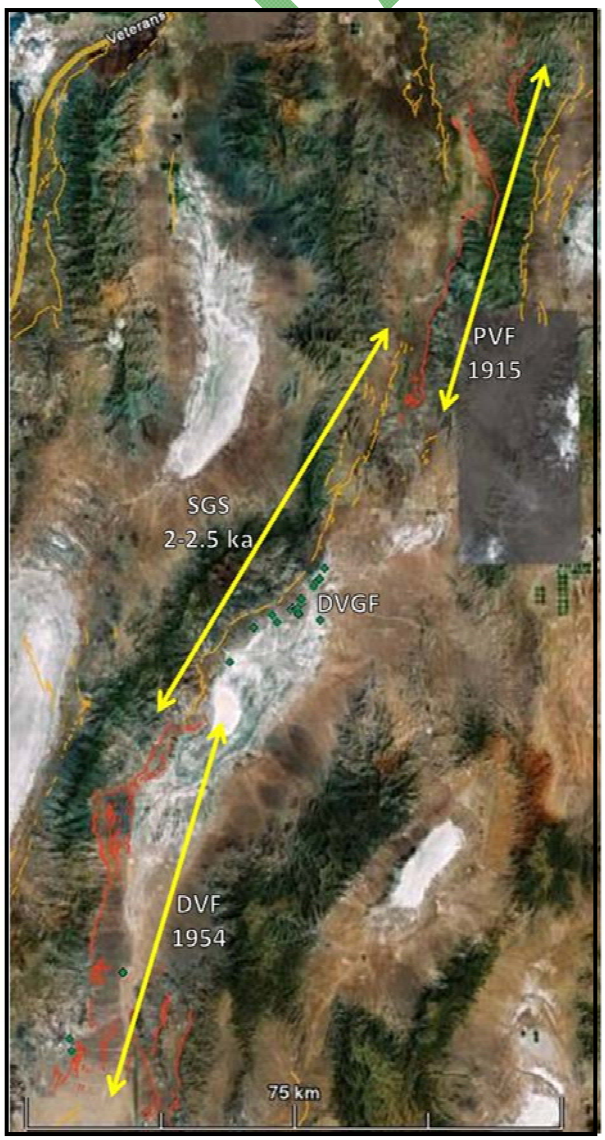

Figure 1 – Map of Dixie Valley region showing approximate location of DVGF (green dots are deep wells within DVGF) in relation to the PVF, SGS, and DVF fault traces (red and orange lines) provided by the USGS Quaternary Fault and Fold Database (QFFDB); see text for definition of the acronyms.

Coulomb 3.1

A numerical code called Coulomb 3.1 can calculate strain and Coulomb Stress Change (CSC) on a receiver fault (RF) due to slip on a source fault (SF) (Lin and Stein, 2004; Toda et al., 2005) in order to determine whether failure along the RF is promoted or inhibited. The first step in using this code is to create an input file containing the spatial boundaries and grid parameters of your model, as well as the appropriate fault parameters (including the starting and ending coordinates, top and bottom depths, dip, slip magnitude and direction) for both the seismogenic SFs and the passive RFs.

Coulomb assumes that a RF (with a specified strike, dip, and rake) exists within each grid cell, and then calculates and plots the strain or CSC value (as resolved onto the RF) at that location. As a result, the location of the RF given in input file does not influence the calculations, but is only used to display the fault on the map/cross section at a particular location of interest.

Scenario 1 *– Reproducing Model from Wesnousky et al. (2003)*

Wesnousky et al. (2003) modeled stress changes on a portion of the SGS as a result of slip on nearby Holocene faults. They represented the DVF as 2 sections and the SGS as 3 sections, but did not include the 1915 event. No evidence exists for a range-front scarp along the SGS section near DVGF, and therefore they suggested this central SGS section *did not rupture* during the "Gap" earthquake. Figure 2A illustrates the calculated change in CSC resolved onto the central SGS fault section (RF) due to slip on the DVF and the 2 other SGS segments (SFs). We use the slip amounts reported in Wesnounsky et al. (2003), and estimate the fault trace lengths and strikes using their Coulomb figure (Figure 2A). SF dips were not reported, so we assign them the same dip used for the RF (50°SE). Fault bottom depths were also not reported, so we assign a fault top and bottom depth of 0 km and 15 km, respectively, based the presence of surface ruptures and the observation that the seismogenic zone over most of the Basin and Range Province extends down to a depth of ~15 km (Smith, 1978). The input parameters used to create our reproduction (Figure 2B) of their figure are given in Table 1.

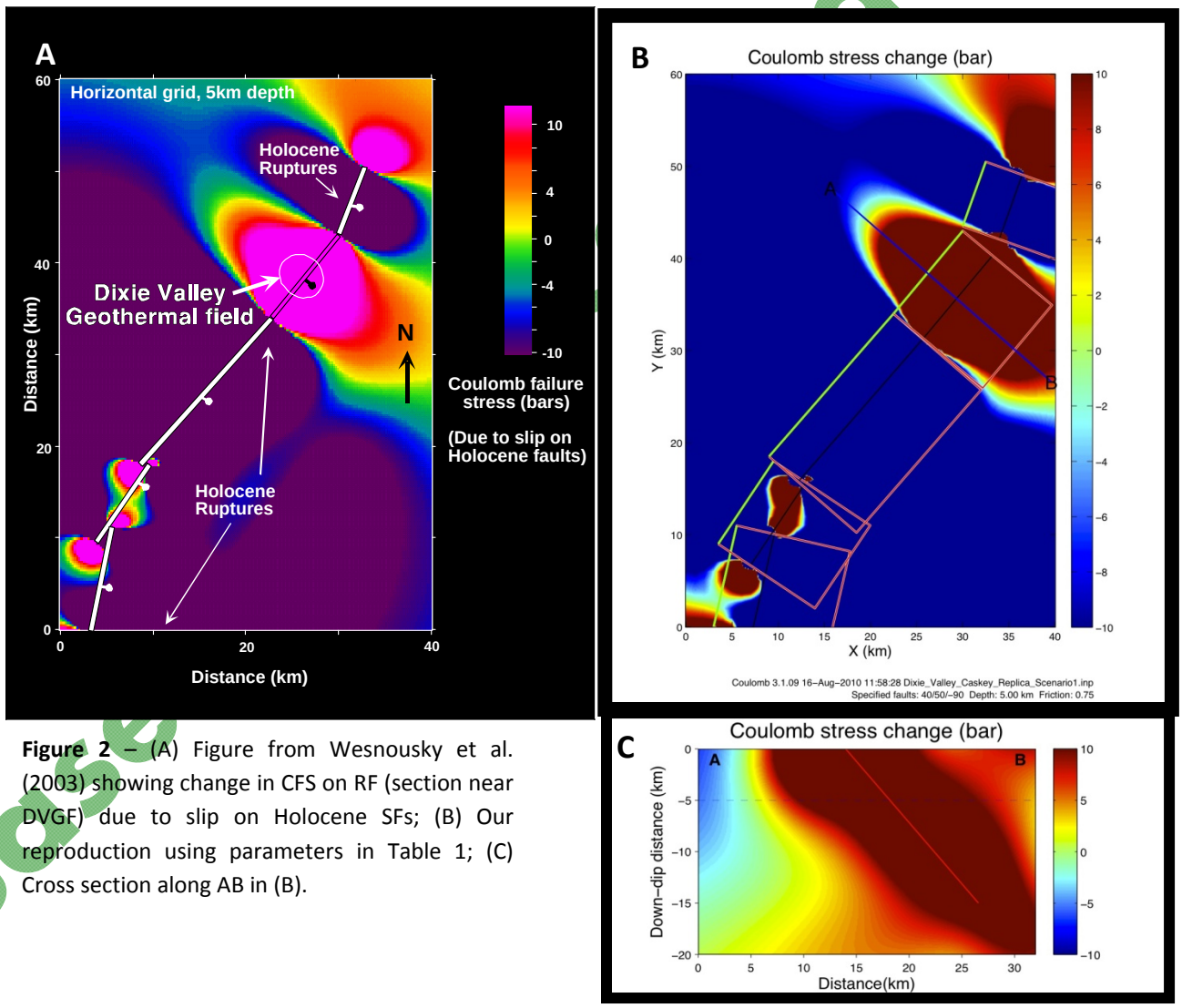

Figure 2 – (A) Figure from Wesnousky et al. (2003) showing change in CFS on RF (section near DVGF) due to slip on Holocene SFs; (B) Our reproduction using parameters in Table 1; (C) Cross section along AB in (B).

Table 1 – Input fault parameters for Scenario 1.

Fault	Segment (SF or RF)	Start x (km)	Start y (km)	End x (km)	End y (km)	Slip (m)	Dip (° SE)	Top (km)	Bottom (km)
SGS	North section (SF)	30	43.5	32.5	50.5	1.96	50	0	15
SGS	Middle section (RF)	22.5	34	30	43	0	50	0	15
SGS	South section (SF)	9	18.5	22.5	34	3.92	50	0	15
DVF	North section (SF)	3.5	9	9.5	18	2.21	50	0	15
DVF	South section (SF)	3	0	5.5	11	1.56	50	0	15

Scenario 1 Discussion

Assuming the middle SGS fault segment (RF) did not rupture 2-2.5 ka, figure 2 illustrates that failure (normal faulting) is promoted on the RF by slip resulting from Holocene ruptures, along with all other faults/cracks with the same orientation (strike, dip, rake) that fall within a region of positive CSC.

Hickman et al. (1998; 2000) suggest that the necessary conditions for high reservoir permeability are that both the local state of stress and orientation of the fault zone be such that the fault is critically stressed for frictional failure (i.e., Sh_{min} is both low and perpendicular to fault). This conclusion is based on stress orientations and magnitudes measured from well-bores (Hickman et al., 1998; 2000; see Table 2) that indicate the fault zone near producing wells of DVGF (73B-7 and 74-7) is critically stressed for normal failure, while the zone near non-producing wells (66-21 and 45-14) is not critically stressed for failure. This is consistent with CSC shown in Figure 2 because productive and non-productive wells fall within zones of positive (failure promoted) and negative (failure inhibited) CSC, respectively (Figure 3).

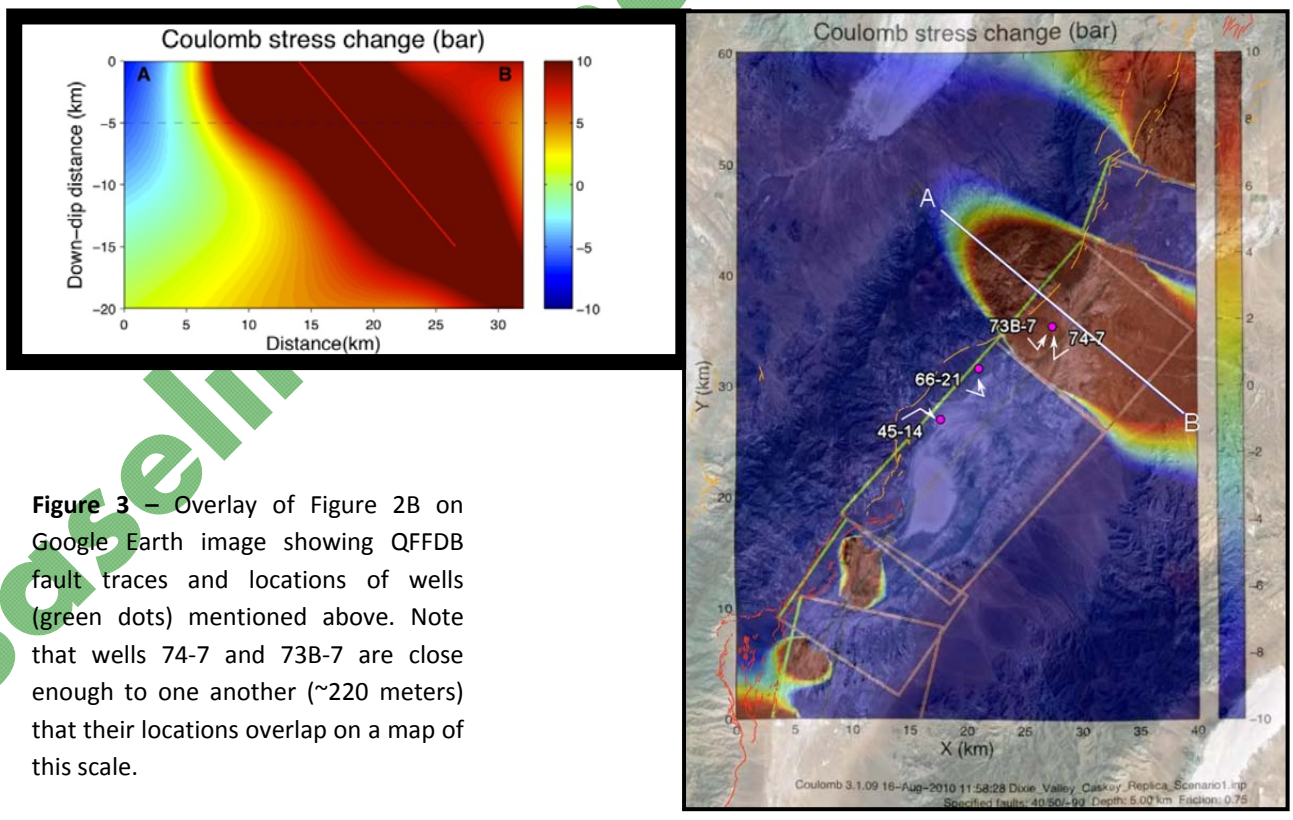

Figure 3 – Overlay of Figure 2B on Google Earth image showing QFFDB fault traces and locations of wells (green dots) mentioned above. Note that wells 74-7 and 73B-7 are close enough to one another (~220 meters) that their locations overlap on a map of this scale.

Table 2 – Information from deep wells penetrating the fault zone at 2-3 km depth. Red and blue indicate critically stressed and not critically stressed well sites (Hickman et al., 1998; 2000).

Well	Sh_{min}	Sh_{min}/Sv	Productive	Interpretation	Scenario 1
73B-7	N57W±10	0.45-0.62 @ 0.4-2.5 km	Y	SFZ optimally oriented and Shmin low (**critically stressed**)	Consistent with well data
74-7	N52W	not reported	Y	SFZ optimally oriented and Shmin low (**critically stressed**)	Consistent with well data
66-21	N20W±20	0.55-0.64 @ 1.9–2.2 km	N	SFZ optimally oriented BUT Shmin high (**not critically stressed**)	Consistent with well data
45-14	N41W±12	0.55-0.64 @ 1.9–2.2 km	N	Shmin low BUT SFZ not optimally oriented (**not critically stressed**)	Consistent with well data

Scenario 2 *– AltaRock Model*

As opposed to Scenario 1, Blackwell et al. (2005) postulated that the whole SGS *did rupture* in the "Gap" earthquake, and suggested that the scarp may have been confined to the range block near the DVGF, i.e. the lack of scarps is not significant. In addition to the main range-front fault, Dixie Valley also contains many piedmont and intrabasin faults of varying orientations. These structures are important to consider because several faults intersect or closely interact with each other in the area of the producing reservoir (Smith et al., 2001), and it has been suggested that none of the production wells in the geothermal field (located 2-3 km into the valley) produce from the exposed main strand of the DVF, but from blind valley (piedmont) segments (Blackwell et al., 2005). For Scenario 2, we represent the DVF as 1 section, the SGS as 3 sections (although not the same sections as Scenario 1), and unlike Scenario 1, we also include the PVF as 1 section. For the three large earthquakes previously discussed, several slightly varying fault orientations and slip magnitudes are suggested from multiple sources (e.g., Blackwell et al., in prep; Caskey et al., 1996; Caskey and Wesnousky, 1997; Smith et al., 2001; Caskey and Wesnousky, 2002; Caskey and Ramelli, 2004; UGSG Quaternary Fault and Fold Database (QFFDB)). The input values (Table 3) used to produce the model for Scenario 2 are based on the following information:

- *1915 Pleasant Valley Earthquake along PVF*
  - Max vertical/horizontal displacements are **5.8m**/**2m**, respectively (Wallace, 1980; 1984)
  - Dip varies from **47-65° NW** (QFFDB)

- *2-2.5 ka "Gap" Earthquake along SGS*
  - Max vertical displacement of **5m** (Caskey and Ramelli, 2004)
  - Dips to the SE, but no angle reported by QFFDB; Blackwell et al. (in prep) suggests dips **70-80° SE** down to at least 3km

- *1954 Dixie Valley Earthquake along DVF*
  - Max vertical displacement of **2.8m** (Caskey et al., 1996)
  - Dip varies from **30-80° SE** (QFFDB)

According to stress orientations and magnitudes presented by Hickman et al. (1998, 2000), the dominant population of permeable fractures within the fault zone near the DVGF is subparallel to the main fault, striking roughly NE and dipping 40-75 degrees SE, with a conjugate set striking roughly the

same direction but dipping NW. Field observations suggest that roughly N-S oriented normal faults are also present (T. Cladouhos, personal communication, 2010) and may play a role within the DVGF. To be consistent with these observations, we explore three different types of RFs: (a) synthetic normal fault subparallel to SGS dipping 70°E, (b) antithetic normal fault subparallel to SGS dipping 70°W, and (c) normal fault oriented roughly N-S dipping 70°W. For each RF, we present figures showing the CSC and dilatational strain in both map and cross-sectional view (Figures 4-6). Please note that all dilatational strain figures are identical (because they are based on same slip amounts on the same SFs), but we chose to include them all in order to display the location of an example RF within the dilatational strain field.

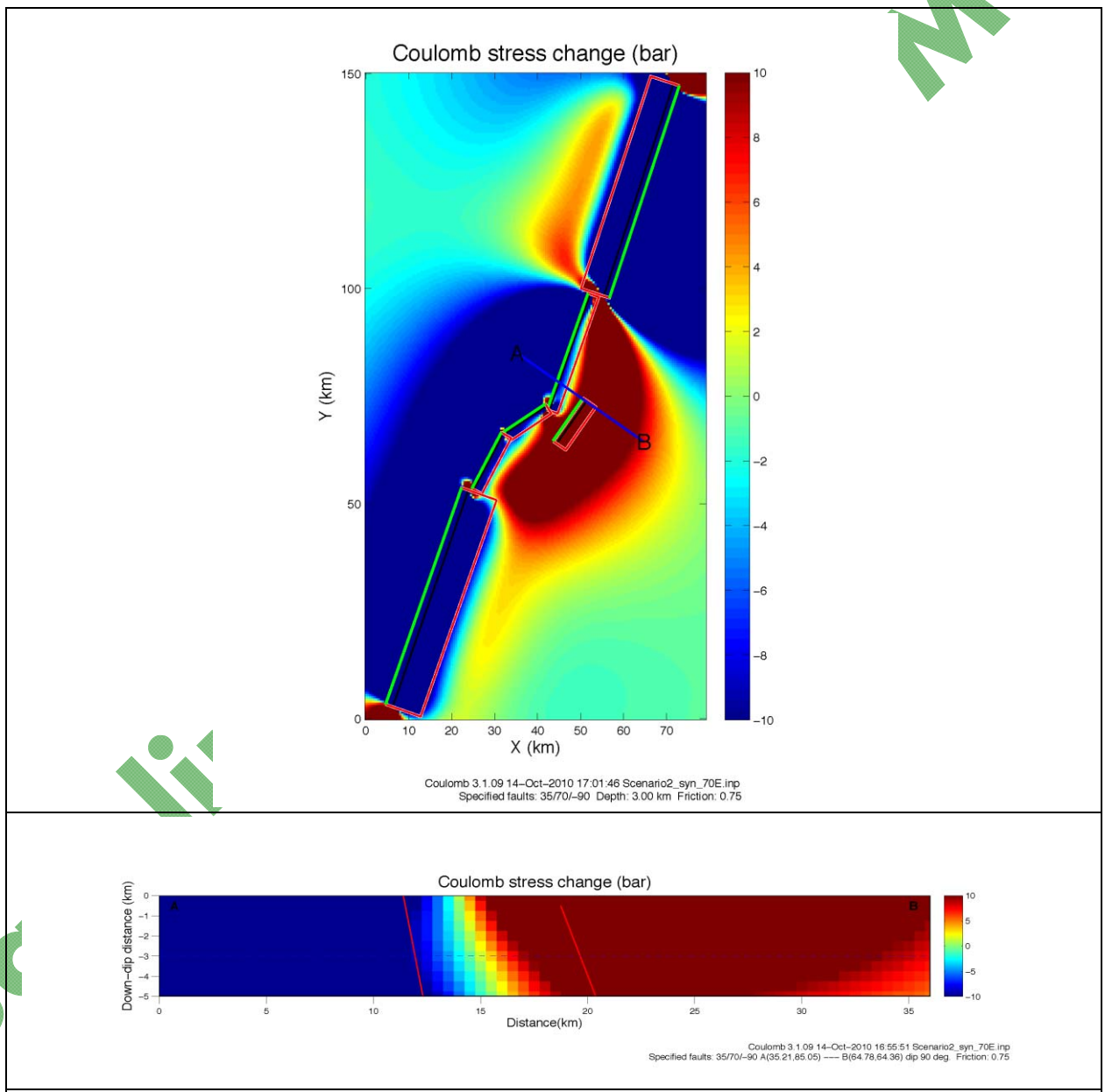

Figure 4(a) – CSC map (top) and cross-section (bottom) of Scenario 2(a) showing CSC resolved onto synthetic RF dipping 70°E due to slip on SFs.

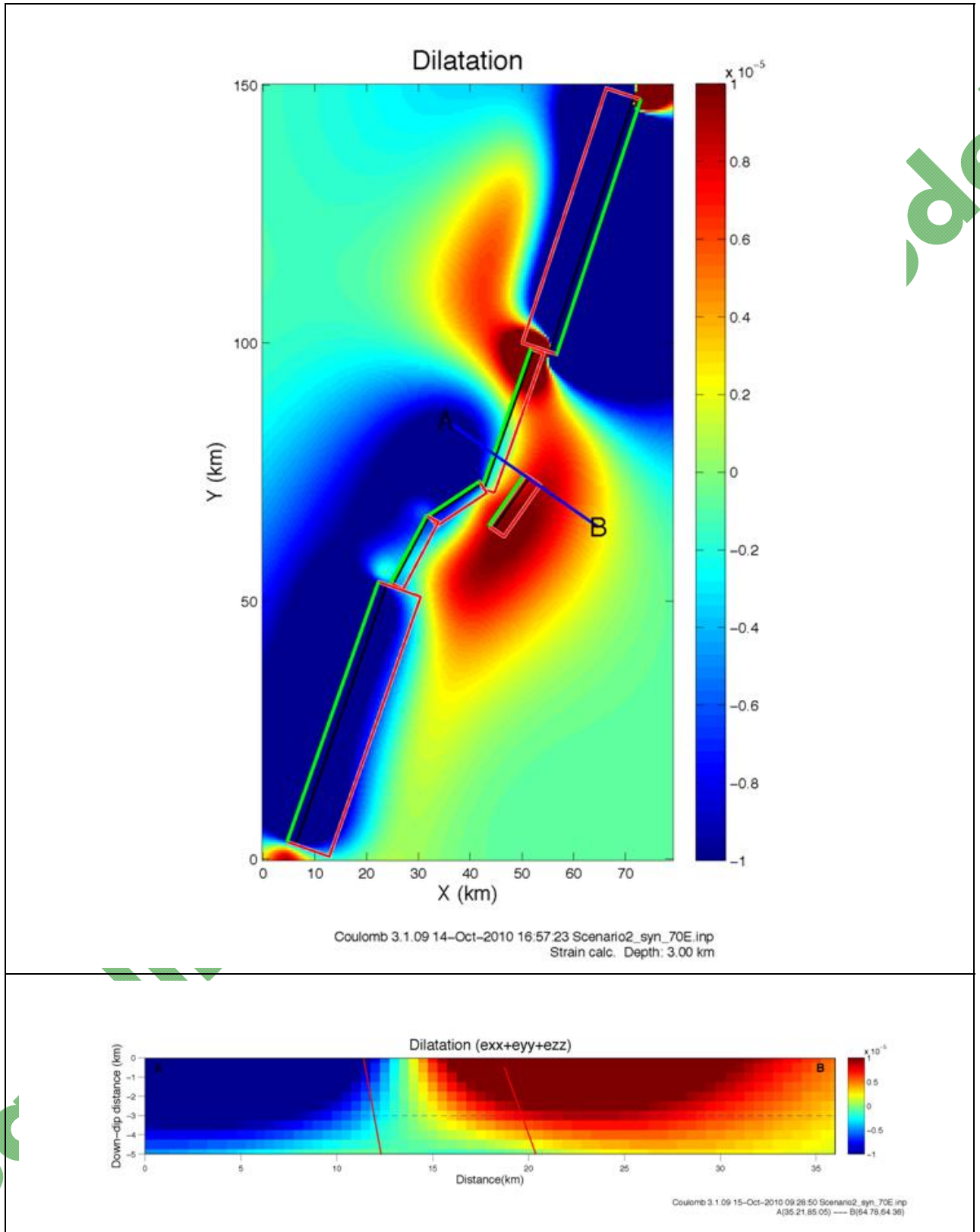

Figure 4(b) – Map (top) and cross-section (bottom) of Scenario 2(a) showing dilatation resolved onto synthetic RF dipping 70°E due to slip on SFs.

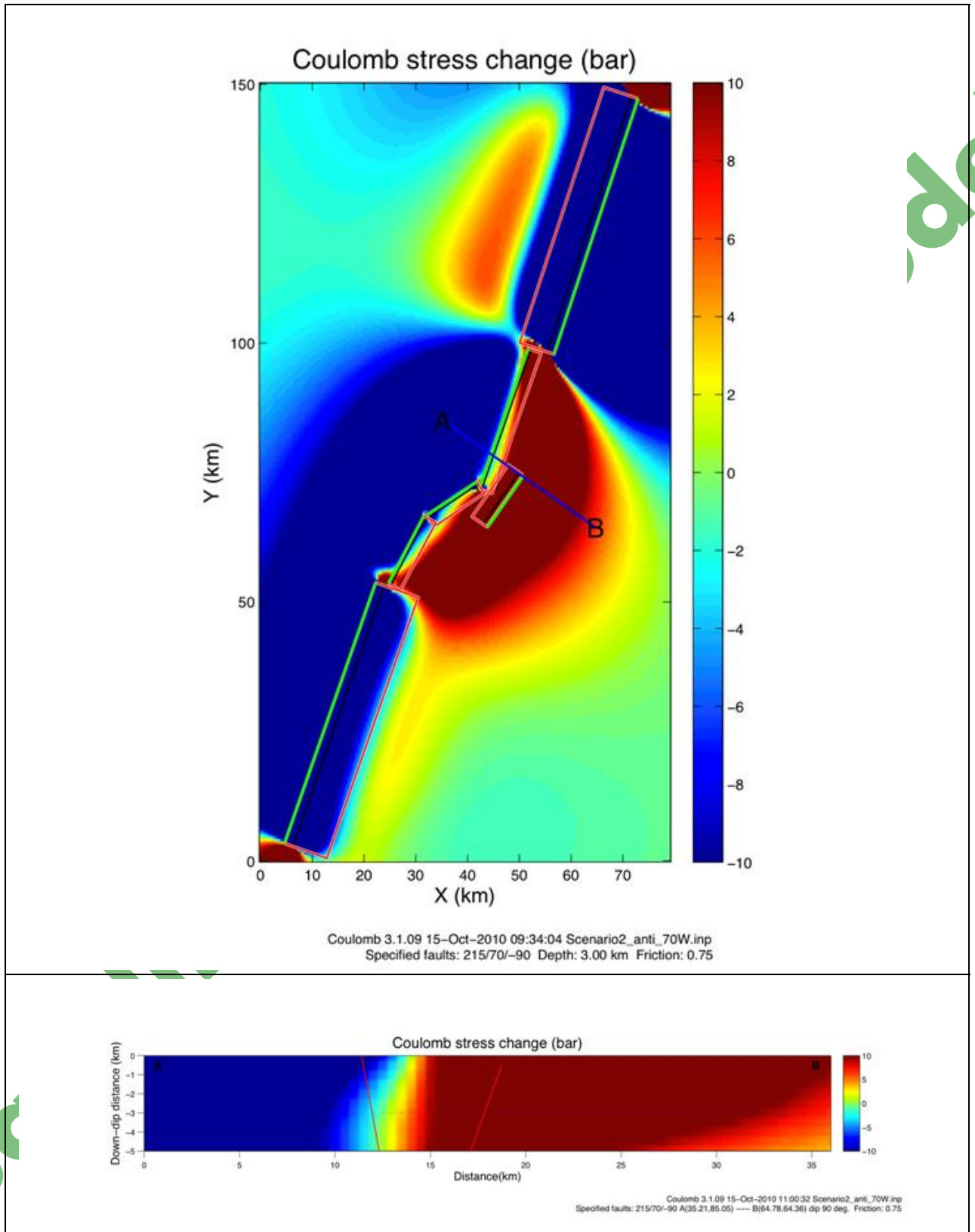

Figure 5(a) – Map (top) and cross-section (bottom) of Scenario 2(b) showing CSC resolved onto antithetic RF dipping 70°W due to slip on SFs.

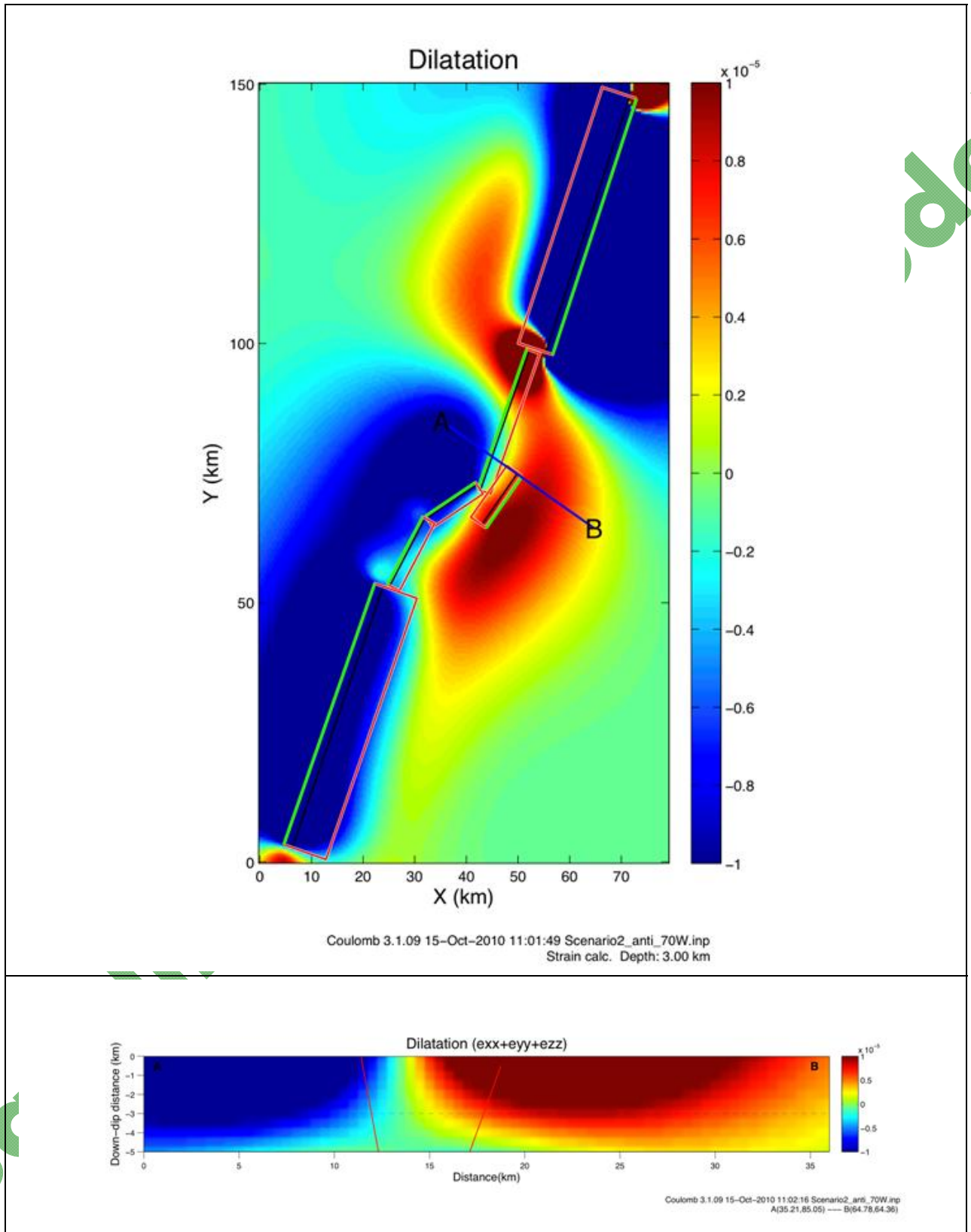

Figure 5(b) – Map (top) and cross-section (bottom) of Scenario 2(b) showing dilatation resolved onto antithetic RF dipping 70°W due to slip on SFs.

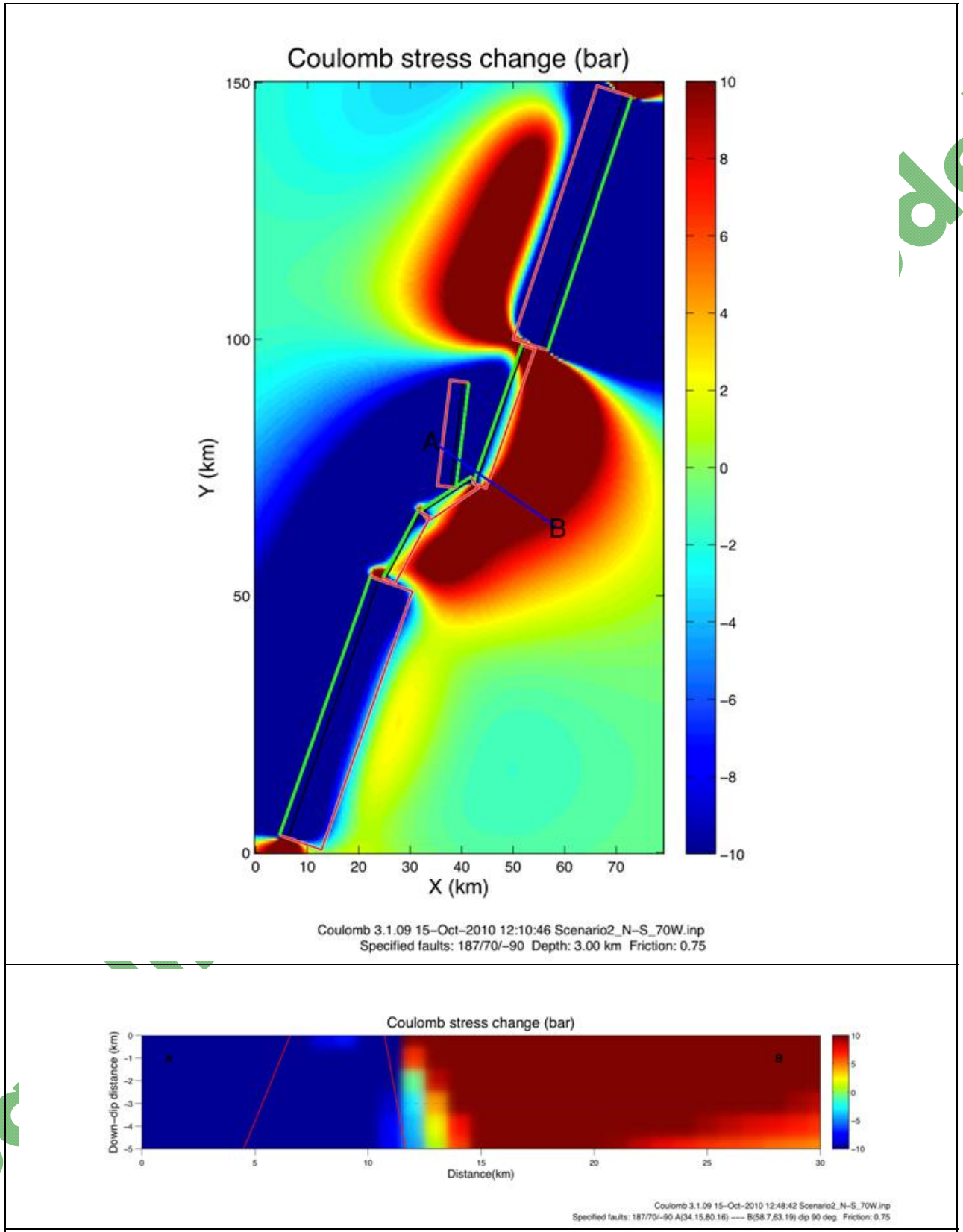

Figure 6(a) – Map (top) and cross-section (bottom) of Scenario 2(c) showing CSC resolved onto N-S oriented RF dipping 70^{o}W due to slip on SFs.

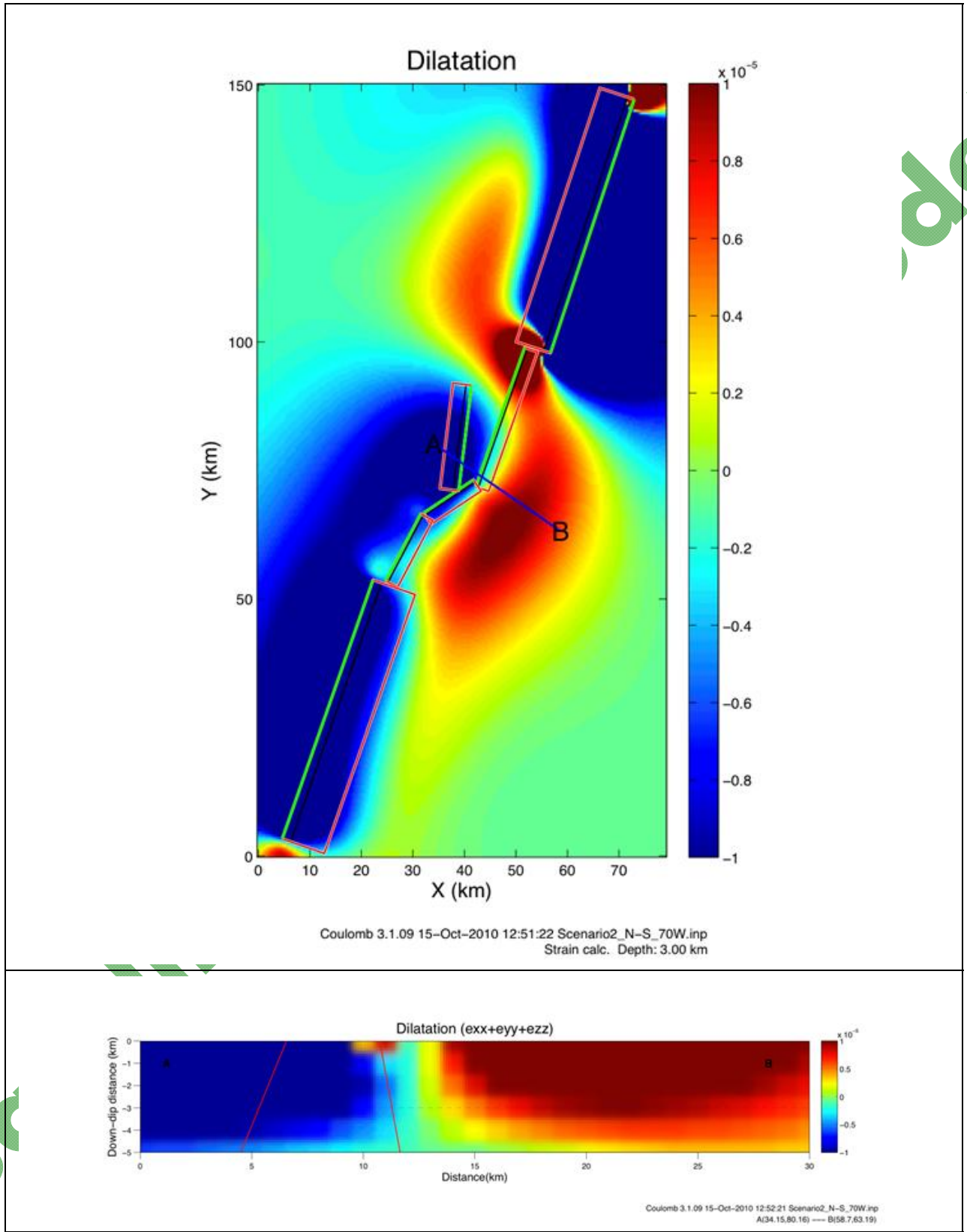

Figure 6(b) – Map (top) and cross-section (bottom) of Scenario 2(b) showing dilatation resolved onto N-S oriented RF dipping 70°W due to slip on SFs.

Table 3 – Input fault parameters for Scenario 2. We estimate the trace lengths and strikes (start and end points) of the PVF, DVF, and SGS using Google Earth surface traces provided by the QFFDB. As in Scenario 1, we assume a fault top and bottom depth of 0km and 15km, respectively, for the SF.

Fault (SF or RF)	Start x (km)	Start y (km)	End x (km)	End y (km)	Slip (m)	Dip (°)	Top (km)	Bottom (km)
1915 PVF (SF)	72.96	147.22	56.71	97.85	5/2 (V/H)	65 W	0	15
2-2.5 ka SGS-North (SF)	42.205	71.843	51.716	98.94	3	80 E	0	15
2-2.5 ka SGS-Middle (SF)	32.066	66.729	41.756	73.189	3	80 E	0	15
2-2.5 ka SGS-South (SF)	24.708	53.539	31.528	66.549	3	80 E	0	15
1954 DVF (SF)	4.63	3.34	22.28	53.71	2	60 E	0	15
(a) synthetic fault (RF)	43.7	64.49	50.7	74.49	0	70 E	0	10
(b) antithetic fault (RF)	50.7	74.49	43.7	64.49	0	70 W	0	10
(c) N-S fault (RF)	41.398	91.583	38.885	71.036	0	70 W	0	10

Scenario 2 Discussion

Assuming that the whole SGS fault segment ruptured 2-2.5 ka (in addition to the 1954 DVF and 1915 PVF ruptures), these figures illustrate that the region near the DVGF lies within a zone of positive CSC and dilatation, and therefore we suggest that slip resulting from these Holocene ruptures promotes normal faulting on all three types of RFs.

As previously mentioned, the fault zone near producing wells of DVGF (73B-7 and 74-7) is critically stressed for normal failure, while the zone near non-producing wells (66-21 and 45-14) is not critically stressed for failure (Hickman et al., 1998; 2000). Figure 7 illustrates that for synthetic RFs dipping 70°E (representative of the dominant set of permeable fractures), the distribution of CSC and dilatational strain is consistent with this observation where productive wells locate within zones of positive CSC (failure is promoted) and dilatation (fault is unclamped), and non-productive wells fall within regions of negative CSC (failure is inhibited) and compression (fault is clamped). Again, the dilatational strain distribution is identical for all three RFs and so we only include it within Figure 7. Figure 8 illustrates that for both antithetic and roughly N-S trending RFs dipping 70°W (representative of the conjugate set of permeable fractures and the N-S oriented faults observed in the field, respectively), the distribution of CSC is also consistent with this observation where productive wells locate within zones of positive CSC (failure is promoted), but is inconsistent where non-productive wells locate within zones of slightly positive CSC. It is worth noting that although a positive CSC value acts to promote failure, the magnitude of CSC is smaller at non-producing wells than producing wells. It may be that productivity at 66-21 and 45-15 is more strongly *inhibited* by compression than *enhanced* by positive CSC (Figure 7). It is worth noting that our modeled fault locations do not coincide exactly with the actual fault locations, and because non-productive wells locate very closely to the transition from positive to negative CSC, this slight difference in fault location could result in non-productive wells plotting within the zone of slightly positive CSC when they are actually located within a zone of negative CSC.

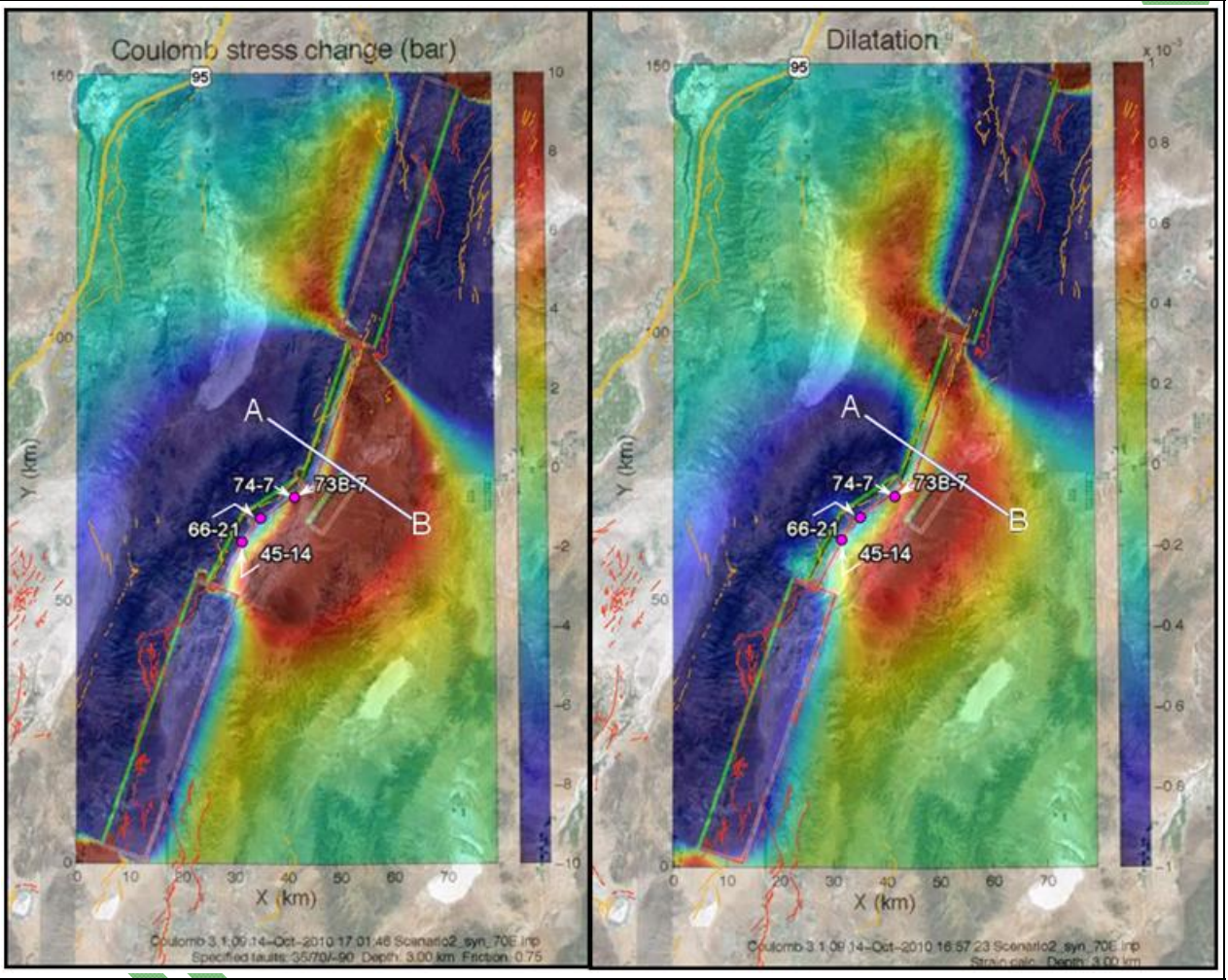

Figure 7 – Overlay of CSC (left) and dilatation (right) maps from Figure 4(a) and (b) on Google Earth image showing QFFDB fault traces and locations of deep wells (magenta dots) mentioned above. Note that wells 74-7 and 73B-7 are close enough to one another (~220 meters) that their locations overlap on a map of this scale.

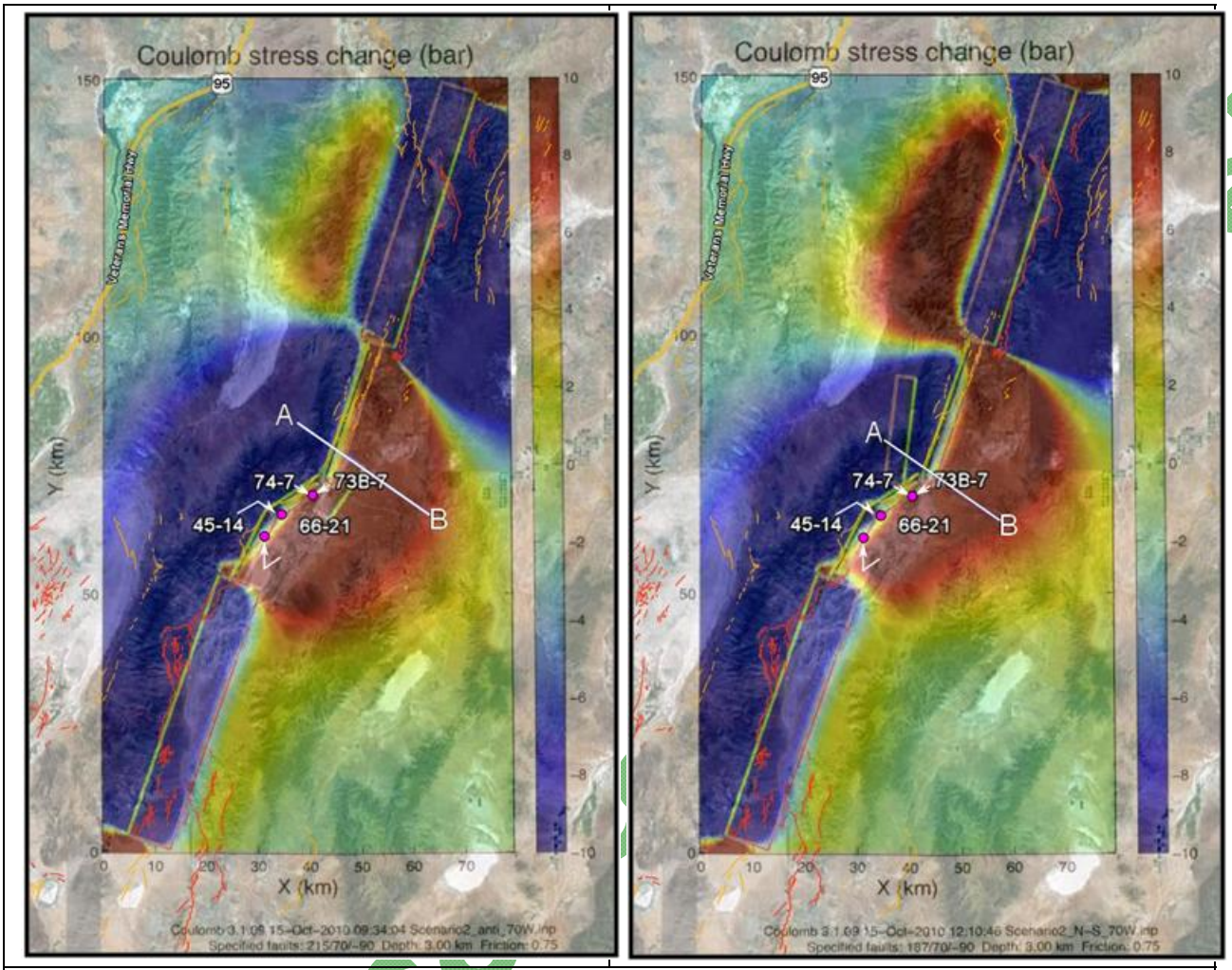

Figure 8 – Overlay of CSC maps from Figure 5(a) and Figure 6(a) on Google Earth image showing QFFDB fault traces and locations of deep wells (magenta dots) mentioned above. Note that wells 74-7 and 73B-7 are close enough to one another (~220 meters) that their locations overlap on a map of this scale.

Table 4 – Information from deep wells penetrating the fault zone at 2-3 km depth. Red and blue indicate critically stressed and not critically stressed well sites (Hickman et al., 1998; 2000).

Well	Sh_{min}	Sh_{min}/Sv	Productive	Interpretation	Scenario 2
73B-7	N57W±10	0.45-0.62 @ 0.4-2.5 km	Y	SFZ optimally oriented and Shmin low (**critically stressed**)	Consistent with well data
74-7	N52W	not reported	Y	SFZ optimally oriented and Shmin low (**critically stressed**)	Consistent with well data
66-21	N20W±20	0.55-0.64 @ 1.9–2.2 km	N	SFZ optimally oriented BUT Shmin high (**not critically stressed**)	Consistent with well data
45-14	N41W±12	0.55-0.64 @ 1.9–2.2 km	N	Shmin low BUT SFZ not optimally oriented (**not critically stressed**)	Consistent with well data

References

Blackwell, D.D., and R. P. Smith, Eds., with contributions from S. Bergman, D. Blackwell, F. Goff, M. Kennedy, J. McKenna, M. Richards, R. Smith, A. Waibel, and P. Wannamaker, 2005. DRAFT Description, Synthesis, and Interpretation of the Thermal Regime, Geology, Geochemistry and Geophysics of the Dixie Valley, Nevada Geothermal System, 191 pp, in review.

Caskey, S.J., Wesnousky, S.G., Zhang, P., and Slemmons, D.B., 1996. Surface faulting of the 1954 Fairview Peak (Ms 7.2) and Dixie Valley (Ms 6.8) earthquakes, central Nevada, Bull. Seismol. Soc. Am., 86, 761-787.

Caskey, S.J. and Wesnousky, S.G., 1997. Static stress changes and earthquake triggering during the 1954 Fairview Peak and Dixie Valley earthquakes, Central Nevada. Bull. Seismol. Soc. Am. 87, 521-527.

Caskey, S.J., and Wesnousky, S.G, 2002. Neotectonics of the Dixie Valley geothermal field and models for late Holocene static stress redistributions. Presentation to Dixie Valley Geothermal Workshop, June 12-13, Reno, Nevada, *http://www.unr.edu/geothermal/oldermeetings.htm*

Caskey, S.J., and Ramelli, A.R., 2004. Tectonic displacement and far-field isostatic flexure from pluvial lake shorelines, Dixie Valley, Nevada, Journal of Geodynamics, 38-2, 131-145.

Hickman, S., Zoback, M., and Benoit, D., 1998. Tectonic Controls on reservoir Permeability in the Dixie Valley, Nevada geothermal field: Proceedings, Twenty-Third Annual Workshop, January 27-28, Geothermal Reservoir Engineering, Stanford Geothermal Program, Stanford, California, 6 p.

Hickman, S. H., Zoback, M. D., Barton, C. A., Benoit, R., Svitek, J. and Summers, R., 2000. Stress and permeability heterogeneity within the Dixie Valley geothermal reservoir: Recent results from well 82-5, Proceedings, 25th Workshop on Geothermal Reservoir Engineering, Stanford University, Stanford, California, January 24-26, SGP-TR-165, p.256-265.

Lin, J. and R.S. Stein (2004), Stress triggering in thrust and subduction earthquakes, and stress interaction between the southern San Andreas and nearby thrust and strike-slip faults, J. Geophys. Res., 109, B02303, doi:10.1029/2003JB002607.

Smith, R.B., 1978. Seismicity, crustal structure, and intraplate tectonics of the interior of the western Cordillera. In: R.B. Smith and G.P. Eaton (Editors), Cenozoic Tectonics and Regional Geophysics of the Western Cordillera. Geol. Soc. Am. Mem., 152: 111-144.

Smith, R.P., Wisian, K.W., and Blackwell, D.D., 2001. Geologic and Geophysical evidence for intra-basin and footwall faulting at Dixie Valley, Nevada, GRC Transactions, 25, 323-326.

Toda, S., R. S. Stein, K. Richards-Dinger and S. Bozkurt, 2005. Forecasting the evolution of seismicity in southern California: Animations built on earthquake stress transfer, J. Geophys. Res., B05S16, doi:10.1029/2004JB003415.

USGS Quaternary Fault and Fold Database of the United States. Fault data updated 20 October 2009. *http://earthquake.usgs.gov/hazards/qfaults/*

Wesnousky, S., Caskey, S.J., and Bell, J.W, 2003. Recency of Faulting and Neotectonic Framework in the Dixie Valley Geothermal Field and Other Geothermal Fields of the Basin and Range, Final Technical Report, University of Nevada, Reno, 26 pp., *http://earthquake.usgs.gov/research/external/reports/08HQGR0027.pdf*